Appl Phys B (2011) 103:597–602
DOI 10.1007/s00340-011-4378-6

Applied Physics B
Lasers and Optics

Optical amplification properties of Dy^{3+}-doped Gd_2SiO_4, Lu_2SiO_5 and $YAl_3(BO_3)_4$ single crystals

P. Haro-González · L.L. Martín · I.R. Martín · M. Berkowski · W. Ryba-Romanowski

Received: 23 July 2010 / Revised version: 8 November 2010 / Published online: 5 February 2011

Abstract Comparative investigation of the optical amplification properties of dysprosium doped Gd_2SiO_5, Lu_2SiO_5 and $YAl_3(BO_3)_4$ single crystals was performed in a pump-and-probe experiment. High power laser pulses at 475 nm were used as the pump source in order to strongly populate the $^4F_{9/2}$ level of the Dy^{3+} ions due to ground state absorption. Low signal beam cw radiation at 574 nm was used as the probe beam to stimulate the emission associated with the $^4F_{9/2} \rightarrow {}^6H_{13/2}$ electronic transition of the Dy^{3+} ions. The process was modelled as a three levels system, and their populations were analysed and simulated in order to study the gain dynamics. Positive optical gain was observed and compared in these crystals. These results confirmed that among the systems studied the Dy^{3+}-doped $YAl_3(BO_3)_4$ single crystal can be considered as a good candidate to develop an optical amplifier employing the $^4F_{9/2} \rightarrow {}^6H_{13/2}$ transition at around 574 nm which is the first step to consider as laser active media.

I.R. Martín, MALTA Consolider Team.

P. Haro-González (✉) · L.L. Martín · I.R. Martín
Dpto. de Física Fundamental y Experimental, Electrónica y Sistemas, Universidad de La Laguna, 38206 La Laguna, Tenerife, Spain
e-mail: patharo@ull.es

M. Berkowski
Institute of Physics, Polish Academy of Sciences, Al. Lotnikow 32/46, 02-668 Warsaw, Poland

W. Ryba-Romanowski
Institute of Low Temperature and Structure Research, Polish Academy of Sciences, Okolna 2, 50-422 Wroclaw, Poland

1 Introduction

Advances in the solid-state laser technology have enabled laser oscillations over wide wavelength regions of UV/VIS and NIR; however, there is still a blank region between 550 and 650 nm, which cannot be covered even with the $Ti:Al_2O_3$ laser and its second harmonic. Within this region, yellow lasers of 560–590 nm have potential applications in a variety of scientific and technological fields especially in the biotechnology [1, 2].

This current interest towards new solid-state visible lasers has led us to carry out a systematic study of the optical amplification possibility in different crystals doped with dysprosium which is the first step to consider as laser active material.

Dy^{3+}-doped materials have been considered as promising laser active materials able to emit radiation associated with the $^6H_{13/2} \rightarrow {}^6H_{15/2}$ transition of Dy^{3+} around 3 μm [3]. Scarce attention was paid to the visible emission originating in the $^4F_{9/2}$ state situated at about 21 000 cm^{-1} [4, 5]. The intense emission in yellow region near 575 nm offers the potential of laser operation since the related transition terminates in the $^6H_{13/2}$ level which is situated well above the ground $^6H_{15/2}$ level.

Compared with other rare-earth ions, there are few reports on optical properties of Dy^{3+}-doped matrices. Kaminskii et al. [6] reported that Dy^{3+}-doped $KGd(WO_4)_2$ and $KY(WO_4)_2$ crystals are promising for directly emitting yellow lasers. Cavalli et al. [7] studied the optical properties of Dy^{3+}-doped $Ba_2NaNb_5O_{15}$(BNN) compounds in order to develop laser media operating in the yellow region as well as white emitting phosphors. A variety of host crystals for Dy^{3+} have subsequently been investigated [8–12]; however, a definitive host crystal for Dy^{3+} has not yet been developed.

In the last years, our research group reported the spectroscopic characteristics of Dy^{3+}-doped Gd_2SiO_5 (GSO) [13],

Lu_2SiO_5 (LSO) [14] and $YAl_3(BO_3)_4$ (YAB) [15–17] single crystals with special attention directed to laser potential associated with the $^4F_{9/2} \rightarrow {}^6H_{13/2}$ transition near 570 nm in the visible. In this work, the results of optical amplification measurements are reported in order to determine the optimal host for visible laser operation from these tree compounds. The gain dynamics of this process is analysed by using the corresponding rate equations that describe the excited state population changes, where a good agreement between the experimental data and the simulation is found.

2 Experimental

2.1 Materials

Single crystals of gadolinium orthosilicate $(Gd_{1-x}Dy_x)_2$-SiO_5 with $x = 0.05$ (GSO) and $(Lu_{1-x}Dy_x)_2$-SiO_5, where $x = 0.05$ (LSO) were grown by the Czochralski method in inductively heated iridium crucible. The starting materials of 99.99% purity were used. They were fired at 1000°C for 4 hours before weighing and mixing. A stoichiometric mixture of Gd_2O_3 and SiO_2 powders for GSO and Lu_2O_3 and SiO_2 powders for LSO were used, as starting materials, in a molar ratio of 1:1. The admixture of dysprosium was doped into above mixture at the content of 5 mol% in place of gadolinium and lutetium, respectively. These materials were put together and then pressed into cylinder tablets under high pressure. The tablets were sintered in a furnace at the temperature of 1500°C for 6 hours before they were loaded into a crucible. Single crystal was grown with convex crystal melt interface on iridium 2 mm rod with pulling rate of 1.5–2 mm/h and speed of rotation 20 rpm [13, 14].

Single crystals of YAl_3 $(BO_3)_4$ (YAB) doped with Dy^{3+} ions (5 mol%) were grown from a $K_2Mo_3O_{10}$ and B_2O_3 flux by spontaneous nucleation using the top-seeded solution growth (TSSG) method [15–17].

2.2 Optical amplification setup

Measurements of optical amplification were carried out in a pump and probe experimental [18–20]. The pump radiation was provided by an optical parametric oscillator (OPO) tuned at 475 nm with high energy pulses between 0.1 and 0.5 J/cm^2 of about 5 ns of duration. The probe beam was obtained by a continuous 400 W lamp together with a monochromator, giving a signal power density of 195 μW/cm^2 at 574 nm with a spectral width of 5 nm.

The incidence of pump and probe beams (linearly polarised) were normal to the surface of the sample (parallel to the c-axis) which was situated after a 1 mm diameter pinhole. A dichroic mirror was employed to align both beams. In order to cover only the whole area of the pinhole, the pump beam was focused with a 20 cm focal length lens.

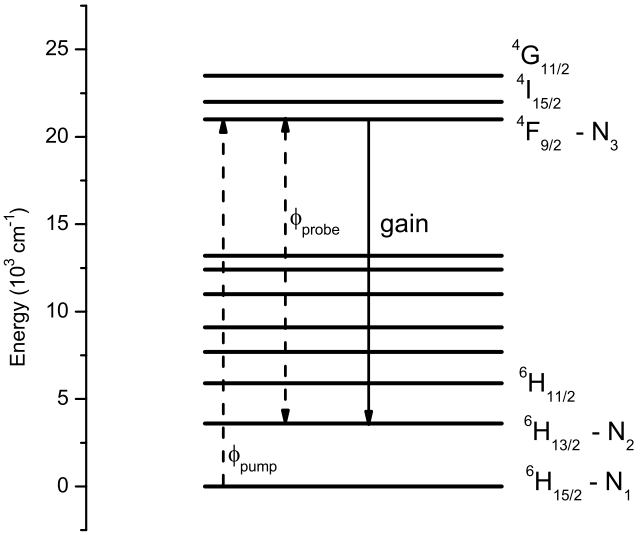

Fig. 1 Energy level diagram of Dy^{3+} ions

The detection chain was formed by a TRIAX-180 monochromator with 1 nm resolution and the output of the photomultiplier tube was registered by a digital oscilloscope TEKTRONIX-2430A for temporal analysis of the decay curves.

To determine the optical gain, two kinds of emission spectra were measured. In the first one, the pump and probe beams were present simultaneously, while the probe was blocked for the second one. Both spectra were compared after subtracting the continuous background due to the probe.

3 Results and discussions

3.1 Theoretical background

The Dy^{3+}:$^6H_{15/2} \rightarrow {}^4F_{9/2}$ Ground State Absorption (GSA) is centred about 475 nm. In the pump and probe experiments, the high power pump pulses at 475 nm induce resonant GSA strongly populating the $^4F_{9/2}$ excited level. In these conditions, a probe beam tuned at 574 nm can induce a relaxation process involving the stimulated emission of a photon at the same frequency. Under this condition, the gain dynamics of this process can be analysed by describing the rate equations of the excited state population changes. A simplified scheme of the levels involved in the process under consideration is shown in Fig. 1. N_i $(i = 1, 2, 3)$ represent the population of the $^6H_{15/2}$, $^6H_{13/2}$ and $^4F_{9/2}$ states, respectively. The rate equations for the populations of the involved levels are:

$$\frac{dN_3}{dt} = \phi_{\text{pump}}\sigma_{\text{ab1}}N_1 - W_3N_3 - \phi_{\text{probe}}(\sigma_{\text{em}}N_3 - \sigma_{\text{ab2}}N_2), \quad (1)$$

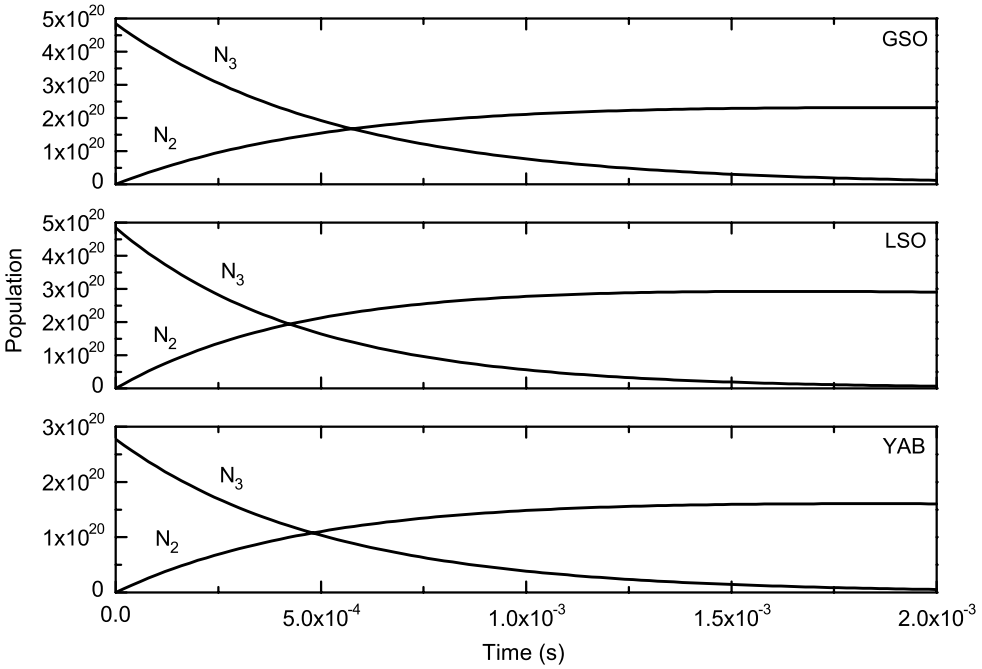

Fig. 2 Simulation of the temporal evolutions of the populations of the $^4F_{9/2}$ (N_3) and $^6H_{13/2}$ (N_2) levels according to the rate equations

Table 1 Radiative branching ratios (b_{ij}), emission (σ_{em}) and absorption (σ_{ab1} and σ_{ab2}) cross-sections and emission radiative relaxation probabilities (W_i) of Dy^{3+} ions in selected hosts

Host	Radiative branching ratios			Cross-section (10^{-20} cm^2)			Emission radiative relaxation probability (s^1)		
	b_{32}	b_{31}	λ_{em}	σ_{em}	σ_{ab1}	σ_{ab2}	W_3	W_2	
GSO	0.54	0.27	569.1	1.21	0.15	1.66	1845	65	[13]
LSO	0.68	0.18	574.3	0.74	0.17	0.81	2158	72	[14]
YAB	0.64	0.17	575.5	1.90	0.26	1.89	1969	59.83	[15]

$$\frac{dN_2}{dt} = W_3 b_{32} N_3 - W_2 N_2 + \phi_{probe}(\sigma_{em} N_3 - \sigma_{ab2} N_2), \quad (2)$$

$$\frac{dN_1}{dt} = -\phi_{pump}\sigma_{ab1} N_1 + b_{31} W_3 N_3 + W_2 N_2. \quad (3)$$

The number of ions removed from ground state by the pump beam is expressed as $\phi_{pump}\sigma_{ab1}N_1$ where σ_{ab1} is the absorption cross-section at 475 nm, σ_{ab2} is the absorption cross-section at 574 nm corresponding to the transition $^6H_{13/2} \rightarrow {}^4F_{9/2}$ and ϕ_{pump} is the incident pumping flux. W_3 and W_2 is the radiative relaxation probability for the N_3 and N_2 levels, respectively, and b_{ij} are the radiative branching ratios. The value of stimulated emission produced by the probe beam is expressed as $\phi_{probe}\sigma_{em}N_3$ where σ_{em} is the emission cross-section of the $N_3 \rightarrow N_2$ and ϕ_{probe} is the flux of the probe beam. The temporal evolution of the gain has been simulated with the help of these rate equations. Due to the pulse of the pump beam, Dy^{3+} ions are excited from the ground state N_1 to the upper state N_3. Then, population inversion for $^4F_{9/2} \rightarrow {}^6H_{13/2}$ transition is expected at $t = 0$ s (immediately after the pump pulse) because $^6H_{13/2}$ is not initially populated. The large energy gap from the $^4F_{9/2}$ to the next lower energy level, around 7000 cm^{-1} [13–15], prevents high multiphonon deexcitation. Therefore, radiative relaxation of this level is expected.

The rate equations (1), (2) and (3) are a set of coupled differential equations that have no analytical solution and, therefore, they have been numerically solved in order to simulate the optical amplification process. The parameters used for each sample are shown in Table 1. The values of the radiative relaxation probabilities, the radiative branching ratios and the emission cross sections are obtained from [13–15]. The values of absorption cross sections at the probe wavelength (574 nm) are calculated by using the McCumber formula [18, 19] where the frequency of the zero-phonon transition between the lowest Stark sublevels of the involved states are obtained from [13–15]. The flux of the probe have been measured experimentally and the obtained value is $\phi_{probe} = 195$ μW/cm^2.

Figure 2 shows the simulated temporal evolution of the N_2 and N_3 levels as a function of the time. At the initial time, N_3 is populated due to GSA and there are not any ions in the N_2 state. Then, N_2 increases due to the ions that decay from N_3, and according to (2) it is due to the spontaneous and stimulated emission contributions. However, the changes inversion densities due to the stimulated emission contribution

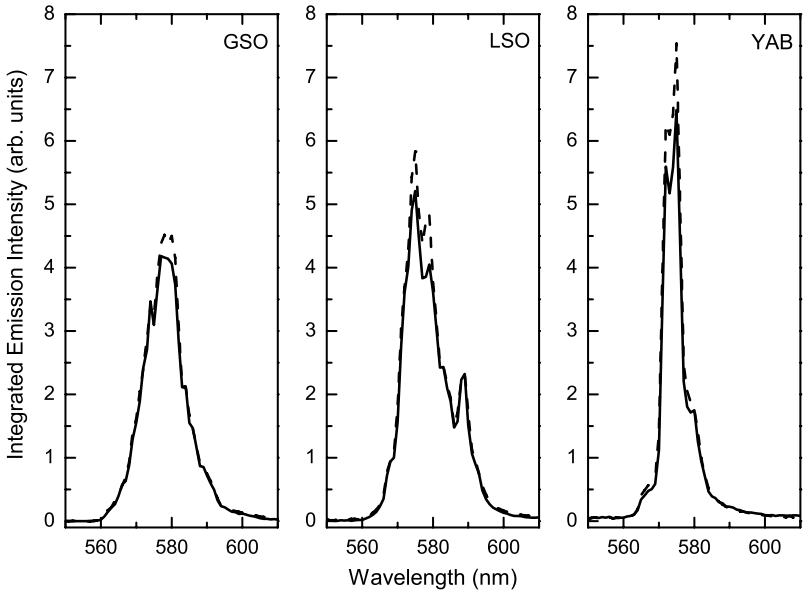

Fig. 3 Emission spectra for Dy^{3+} doped GSO, LSO and YAB crystals at 574 nm probe wavelengths. The *solid line* corresponds to I_p and the *dashed line* shows I_{pp}

Table 2 Concentration of Dy^{3+} ions (N_T), theoretical maximum gain (g_{max}) and experimental gain (g_{exp})

	N_T (10^{20} ions/cm^3)	$g_{max} = \sigma_{em}N_3 - \sigma_{ab2}N_2$	g_{exp}
GSO	4.84	5.85	3.49
LSO	4.84	3.58	3.39
YAB	2.77	5.26	3.96

are nearly negligible in this simulation. The gain coefficient can be related to the N_3 and N_2 populations through the expression:

$$g = \sigma_{em}N_3 - \sigma_{ab2}N_2. \tag{4}$$

According to (4), positive optical gain is expected when the value of $\sigma_{em}N_3$ is higher than $\sigma_{ab2}N_2$. An estimation of the maximum optical gain that can be achieved between the Dy^{3+}:$^4F_{9/2}$ and the $^6H_{13/2}$ levels have made with (4). Using the values given in Table 1, the theoretical maximum optical gain is given in Table 2.

3.2 Experimental results

As mentioned in the experimental section, two emission spectra were recorded: the first one with pump and probe present and the second one with the probe blocked. These spectra are given in Fig. 3. An increase of the detected intensity at the probe wavelength can be clearly appreciated. This increment is due to the stimulated emission associated with the $^4F_{9/2} \rightarrow {}^6H_{13/2}$ transition that occurs at the probe wavelength and it is the physical basis of signal amplification. Moreover, to corroborate that this enhancement of the emission is due to the probe beam, the wavelength of the probe beam was shifted from 574 nm to the sides of the spectrum and it was found that the intensity enhancement was shifted accordingly to the signal wavelength. However, when the probe beam was shifted outside of the emission band there were no changes in the emission spectrum. Under this pumping scheme, the maximum population inversion for $^4F_{9/2} \rightarrow {}^6H_{13/2}$ transition at 574 nm is expected at $t = 0$ s (immediately after the pump pulse) because $^6H_{13/2}$ is not initially populated. Moreover, the optical gain is estimated to have duration according to the lifetime of this level, in good agreement with the previous simulation.

The optical gain in the sample has been estimated by taking into account the following considerations. When a probe beam passes through a solid medium, its intensity decreases from the initial I_0 value to the final $I_{probe}(L)$ value according to the exponential law (for low intensities):

$$I_{probe}(L) = I_o e^{-\alpha L}, \tag{5}$$

where α and L are the absorption coefficient and the length of the sample, respectively. When the pump and the signal are simultaneously switched on, and assuming a homogeneous pump along the propagation direction, the intensity recorded after the samples at the signal wavelength, I_{pp}, is given by:

$$I_{pp} = I_p + I_o e^{(g-\alpha)L}, \tag{6}$$

where I_p is the spontaneous emission intensity induced by the pumping radiation and g is the internal gain coefficient. The signal enhancement (SE) is defined as [20–22]:

$$SE = \frac{I_{pp} - I_p}{I_{probe}}. \tag{7}$$

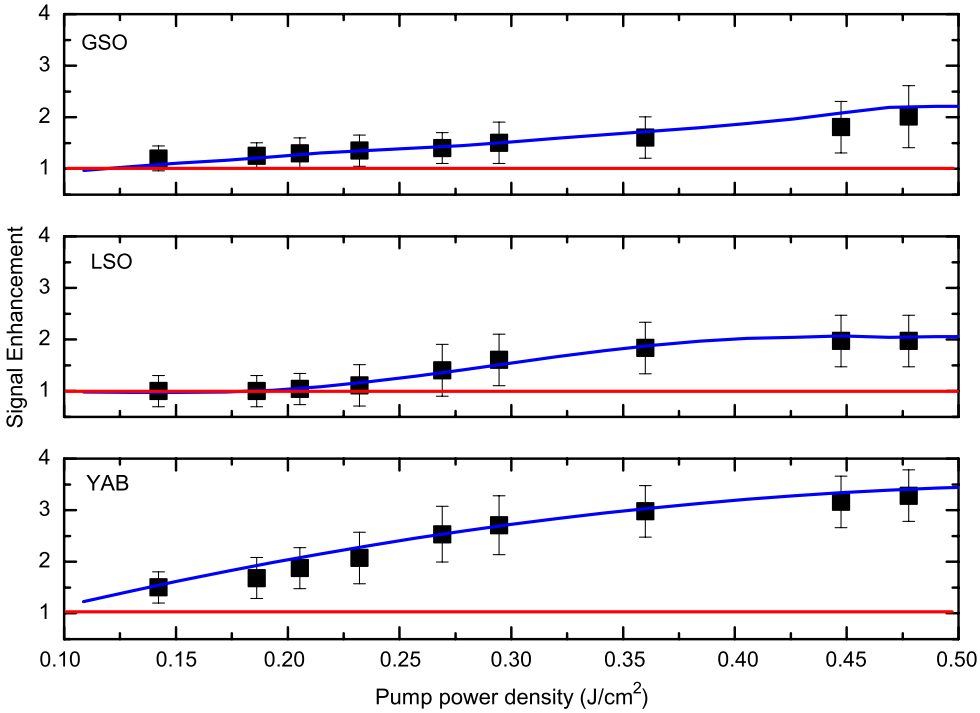

Fig. 4 Signal Enhancement as function of the pump power density for Dy^{3+}-doped crystals. The *red lines* show the limit of positive optical gain coefficient where the SE is higher than 1, and the *blue lines* are a guide for the reader

By introducing (5) and (6) in the expression (7), SE becomes:

$$\mathrm{SE} = \exp(gL). \tag{8}$$

Considering α nearly negligible at 574 nm [13–15], I_{probe} is constant along the sample and (8) is identical to the net gain:

$$\mathrm{SE} = \exp((g-\alpha)L). \tag{9}$$

The intensities I_{p}, I_{pp} and I_{probe} can be experimentally measured, and by using (7) the SE is obtained. The SE as a function of the pump energy density is given in Fig. 4. A continuous growth of the SE as a function of the pump power density can be observed in this figure which corresponds to a continuous growth of the net optical gain. Finally, the net gain coefficient has been obtained by using (9) where the maximum value has been observed for a pump energy density of 0.5 J/cm^2.

The results of this experiment are collected in Table 2, where the theoretical and experimental values of the gain coefficients are included. As can be seen in this table, all the theoretical values are higher than the experimental ones. This result could be explained on the basis of neglected losses (α) at 574 nm in (9).

3.2.1 *GSO crystal*

According to the simulation reported in Fig. 2 and (4), a positive optical gain during the first ~550 μs is expected, in good agreement with the lifetime of this level [13]. By using (4), the theoretical maximum expected gain is 5.85 cm^{-1} (see Table 2). The experimental results of the SE in GSO crystal are given in Fig. 4 where a continuous growth as a function of the pump energy density is found. At the maximum pump energy density available in this set-up, a value for the net gain of 3.49 cm^{-1} is found.

3.2.2 *LSO crystal*

In the case of the LSO crystal, the simulation given in Fig. 2, using (4), shows the possibility of finding positive optical gain during the first ~ 420 μs, giving the maximum value at $t = 0$ s. According to this result, the experimental values obtained for the optical amplification in the LSO crystal are given in Fig. 4. A maximum gain coefficient of 3.39 cm^{-1} is obtained, which is the lowest value obtained at the highest pump energy density available in this set-up. Moreover, there is a threshold to obtain optical amplification at 0.2 J/cm^2 which is a higher threshold when compared with the other crystals. These results are in agreement with the lowest emission cross-section [14] when compared with the other Dy^{3+}-doped crystals (see Table 1).

3.2.3 *YAB crystal*

The YAB crystal shows the maximum gain coefficient obtained under this pumping condition with a value of 3.96 cm^{-1}. Moreover, the experimental threshold to find optical amplification is expected at lower values of pump energy density. A continuous growth of the gain coefficient

is obtained along the allowed pump energy density range. According to the simulation reported in Fig. 2 and (4), positive optical gain can be found during the first ~ 480 µs, in good agreement with the lifetime of this level [15], which supports the proposed excitation mechanism. This highest value of the optical gain and this small threshold can be related to the highest emission cross-section coefficient (σ_{em}) (see Table 1) [15].

4 Conclusions

Positive optical gain was recorded in Dy^{3+}-doped GSO, LSO and YAB single crystals in a pump-and-probe experiment. The hosts were pumped at 475 nm to populate the $^4F_{9/2}$ level of the Dy^{3+} ions. Low signal beam cw radiation at 574 nm was used as the probe beam to stimulate the emission associated with the $^4F_{9/2} \rightarrow {}^6H_{13/2}$ electronic transition of the Dy^{3+} ions. The gain dynamics of this process was simulated as a three levels system and compared with the experimental results; good agreement between the experimental data and the simulation was obtained.

The optical coefficients were recorded for the different Dy^{3+}-doped crystals. At the maximum pump energy density available in this experiment, a gain value of 3.49 cm^{-1} (15.14 dB/cm^{-1}) was found for the GSO, 3.39 cm^{-1} (14.71 dB/cm^{-1}) for the LSO, and 3.96 cm^{-1} (17.18 dB/cm^{-1}) for the YAB crystals.

These results confirmed that among systems studied the Dy^{3+}-doped YAB single crystals can be considered as good candidates to develop an optical amplifier employing the $^4F_{9/2} \rightarrow {}^6H_{13/2}$ transition at around 574 nm which is the first step to consider as laser active media. It is expected that laser amplification could be obtained with a pump power density from 0.15 J/cm^2.

Acknowledgements The authors gratefully acknowledge the financial support of this research by the Comisión Interministerial de Ciencia y Tecnología (MAT2007-65990-C03-02 and MAT2010-21270-C04-02), Malta Consolider-Ingenio 2010 (CSD2007-0045) and FPI grant by Agencia Canaria de Investigación del Gobierno de Canarias.

References

1. M. Bigos, N. Baumgarth, G.C. Jager, O.C. Herman, T. Nozaki, R.T. Stovel, D.R. Parks, L.A. Herzenberg, Cytometry **36**, 36 (1999)
2. W. Telford, M. Murga, T. Hawley, R. Hawley, B. Packard, A. Komoriya, F. Haas, C. Hubert, Cytometry, Part A **68A**, 36 (2005)
3. L.F. Johnson, H.J. Guggenheim, Appl. Phys. Lett. **23**, 96 (1973)
4. W. Ryba-Romanowski, I. Sokólska, G. Dominiak-Dzik, S. Gołąb, J. Alloys Compd. **300**, 152 (2000)
5. W. Ryba-Romanowski, G. Dominiak-Dzik, P. Solarz, R. Lisiecki, Opt. Mater. **31**, 1547 (2009)
6. A. Kaminskii, U. Hömmeric, D. Temole, J.T. Seo, K. Ueda, S. Bagayev, A. Pavlyuk, Jpn. J. Appl. Phys. **39**, L208 (2000)
7. E. Cavalli, A. Belletti, R. Mahiou, P. Boutinaud, J. Lumin. **130**, 733 (2010)
8. S. Zhang, Z. Cheng, Z. Zhuo, J. Han, H. Chen, Phys. Status Solidi A **181**, 485 (2000)
9. E. Cavalli, E. Bovero, A. Belletti, J. Phys., Condens. Matter **14**, 5221 (2002)
10. E. Cavalli, M. Bettinelli, A. Belletti, A. Speghini, J. Alloys Compd. **341**, 107 (2002)
11. Z. Wang, D. Yuan, X. Shi, X. Cheng, D. Xu, M. Lu, L. Pan, J. Cryst. Growth **263**, 246 (2004)
12. D.K. Sardar, W.M. Bradley, R.M. Yow, J.B. Gruber, B. Zandi, J. Lumin. **106**, 195 (2004)
13. R. Lisiecki, G. Dominiak-Dzik, P. Solarz, W. Ryba-Romanowski, M. Berkowski, M. Głowacki, Appl. Phys. B **98**, 337 (2010)
14. G. Dominiak-Dzik, W. Ryba-Romanowski, R. Lisiecki, P. Solarz, M. Berkowski, Appl. Phys. B **99**(1–2), 285 (2010)
15. G. Dominiak-Dzik, P. Solarz, W. Ryba-Romanowski, E. Beregi, L. Kovacs, J. Alloys Compd. **359**, 51 (2003)
16. G. Dominiak-Dzik, W. Ryba-Romanowski, L. Kovacs, E. Beregi, Radiat. Meas. **38**, 557 (2004)
17. W. Ryba-Romanowski, G. Dominiak-Dzik, P. Solarz, R. Lisiecki, Opt. Mater. **31**(11), 1547 (2009)
18. D.E. McCumber, Phys. Rev. **136**(4A), A954 (1964)
19. R. Quimby, J. Appl. Phys. **92**, 180 (2002)
20. P. Haro-González, I.R. Martín, F. Lahoz, S. González-Pérez, E. Cavalli, N.E. Capuj, J. Appl. Phys. **106**, 113108 (2009)
21. P. Haro-González, F. Lahoz, I.R. Martín, S. González-Pérez, F. Rivera, N.E. Capuj, Opt. Mater. **31**, 1370 (2009)
22. P. Haro-González, M. Bettinelli, N.E. Capuj, F. Lahoz, I.R. Martín, E. Cavalli, S. González-Perez, Opt. Mater. **32**, 475 (2010)